Vol. 40, No. 4 (2018) 538-551, DOI: 10.24874/ti.2018.40.04.03

Tribology in Industry

www.tribology.rs

RESEARCH

Viscoelastic Contact Modelling: Application to the Finite Length Line Contact

S. Spinu[a,b]

[a] *Department of Mechanics and Technologies, Stefan cel Mare University of Suceava, 13th University Street, 720229, Suceava, Romania.*

[b] *Integrated Center for Research, Development and Innovation in Advanced Materials, Nanotechnologies, and Distributed Systems for Fabrication and Control (MANSiD), Stefan cel Mare University, Suceava, Romania.*

Keywords:

Finite length line contact
Numerical simulation
Viscoelastic displacement
End effect
Eccentric loading

Corresponding author:

S. Spinu
Department of Mechanics and Technologies, Stefan cel Mare University of Suceava, 13th University Street, 720229, Suceava, Romania.
E-mail: sergiu.spinu@fim.usv.ro

A B S T R A C T

The design of machine elements made by viscoelastic matrix can be improved by numerical analysis. The solution of the viscoelastic contact problem with prescribed geometry is difficult to obtain because (1) both contact area and pressure distribution are a priori unknown, and (2) the contact parameters keep changing with time, together with the compliance of the viscoelastic material. These difficulties are overcome in this paper by conducting numerical analysis based on both spatial and temporal model discretization. The viscoelastic contact process simulation is achieved by computing a series of subsequent contact states, the current state depending on the entire contact history. In this manner, the memory effect of the viscoelastic material is accounted for. The numerical predictions agree well with the classic solution of the spherical contact undergoing step loading. The history of pressure distribution and modification of contact area in the finite length line contact between a rigid profiled roller and a polymethyl methacrylate viscoelastic half-space are obtained. The case when the normal force is applied eccentrically in the longitudinal direction, leading to a tilting moment, is also considered.

© 2018 Published by Faculty of Engineering

1. INTRODUCTION

The reliability of mechanical contacts involving machine elements made by viscoelastic matrix can be extended by numerical analysis. The latter can overcome the limitations existing in most analytical solutions, regarding the constitutive law of the contacting material or the contact geometry, which is usually restricted to axisymmetric cases. The finite length line contact has important applications in the bearing technology, and the stress analysis of cylindrical rolling elements is of major importance, considering that the raceway life was proven [1] to decrease with at least the ninth power of contact stress. Moreover, it is well known [1-3] that small changes in the profile of the rolling element can significantly influence the contact stress. At the moment of the analysis, the relationship between the roller profile and the surface stress cannot be assessed analytically even in the simplest case of linear

and isotropic elastic bodies. The classic solutions of viscoelastic contact analysis [4-8], obtained based on the correspondence principle between the elastic and the viscoelastic problems of stress analysis, are also restricted to axisymmetric contact geometry and therefore cannot be applied in the study of the finite length line contact. Moreover, the mathematical complexity of these partially analytical classic solutions challenges their wide range application. It has been shown [9,10] that a viscoelastic problem has an associated elastic problem, to which the former reduces after removal of time dependency by application of the Laplace transform. The classic concept of associated elastic problem involves removal of time dimension via Laplace transform. In this manner, the viscoelastic problem is reduced to a formally identical elastic problem, whose solution is easier to obtain. If the boundary conditions are time-independent, a solution in the frequency domain is identical in form to the corresponding elastic solution. However, handling the transient boundary conditions encountered in most contact scenarios may be difficult, if not impossible, leading to solutions of limited viability.

The indentation of a viscoelastic half-space by a rigid indenter features time-dependent boundary conditions. The first tentative solution was obtained [4] by replacing the elastic constant in the solution of the associated elastic problem with the appropriate integral or differential viscoelastic operator. Applied to spherical indentation, the latter technique lead to solutions that hold true as long as the contact radius increases monotonically with time. A more versatile solution was later obtained by Ting [7,8], allowing for any number of loadings and unloadings, on consideration of up to six possible cases based on the loading history. The latter solution cannot be considered explicit, as it involves solution of transcendental equations.

An alternative approach, more suited to the numerical treatment of the viscoelastic contact problem, consists in constructing a sequence of elastic contact problems with boundary conditions that are matched exactly to those of the viscoelastic contact problem at a series of specified times. This approach is based on the fact that, provided the compatibility and internal equilibrium equations are satisfied instantaneously, any elastic solution to a problem becomes an instantaneous viscoelastic solution. Recent research efforts [11-13] in the field of numerical analysis of bodies with arbitrary geometry and complex rheological behavior may provide an important starting point for the understanding of the viscoelastic contact involving complex contact geometries. The numerical approach is based on the fact that, unlike its counterpart [4] expressing the contact radius, the displacement equation obtained by replacing the elastic constant in the solution of the associated elastic problem with the integral or differential viscoelastic operator, does not require additional manipulations and can be used in conjunction with any history of boundary conditions.

In this paper, the finite length line contact of linear viscoelastic materials is simulated numerically using a technique originally developed for the elastic contact of rough bodies [14], combined with a method for viscoelastic displacement computation [15]. The resulting contact model can predict the pressure distribution, the end effect and the force eccentricity outcome in the finite length line contact of linear viscoelastic materials with arbitrary loading history and complex rheological behavior.

2. CONTACT MODEL

The contact model employed in this paper is an extended version of the framework adopted in [14]. The increase in generality stems from consideration of a tilting moment susceptible to arise in conforming or line contacts, in which the normal force is applied eccentrically. In such cases, the resultant of the induced pressure is not aligned with the contact normal axis. The contact problem is described in a Cartezian coordinate system, with the x_1 and x_2 axes laying in the common plane of contact, i.e. the plane that separates best the limiting surfaces of the contacting bodies. The mathematical model consists in three type of equations: (1) the equation of the surface of deformation between the two bodies, (2) the boundary conditions, and (3) the static equilibrium. The latter equation comprises both normal force and tilting moment equilibrium equations, meaning the force eccentricity effect can be properly simulated.

However, as the contact is assumed frictionless, no shear stresses can be supported by the contact interface, and consequently no tangential force or spin moment is considered in the equilibrium equations.

The equation of the clearance between the contacting bodies, measured along the normal direction x_3, stems from comparison of the contact geometry before and after the elastic deformation required to accommodate the transmitted load. The so-called condition of deformation can be expressed as:

$$h(x_1, x_2) = hi(x_1, x_2) + u_3(x_1, x_2) - \omega - \alpha x_1, \quad (1)$$

where h denotes the gap between the deformed bodies, hi the initial gap (in unloaded state), u_3 the composite (i.e., relative) displacement along the x_3-axis, ω the rigid-body approach, and α the tilting angle due to the normal force eccentricity in surface contacts. It should be noted that the latter parameter, as well as the normal approach ω, are rigid-body movements that are measured between points and directions in the contacting bodies distant from the contact region, which is subjected to deformation.

Without losing generality, the force eccentricity is allowed along the x_1-axis (matching the line contact longitudinal direction), leading to a tilting moment about the x_2-axis. This simplifying assumption is well suited to finite-length line contacts. Any force eccentricity along the transverse direction would cause rolling, which is beyond the point of this study.

The boundary conditions and constraints are the mathematical expression of other two assumptions: (1) non-negativity of pressure, and (2) impenetrability of the bodies. The first assumption leads to neglect of contact adhesion, and can be considered conservative in the case of adhesive contacting material. However, this assumption is required to obtain the pressure distribution by the classic minimization process, seeking the minimum of a quadratic form, i.e. the complementary energy, subjected to constraints, i.e. the boundary conditions, as described in [16]. It should be noted that this assumption is common in the literature of the viscoelastic contact. The classic viscoelastic solution [4-8] is obtained by considering a surface displacement compatible with the indenter profile within the contact area. Such an assumption can not guarantee that contact tractions are everywhere compressive. Consequently, no step back is made in the model proposed in this paper, and the influence of adhesion in viscoelastic contacts is left for further research efforts.

The second assumption involves the non-negativity of the clearance between the contacting surfaces, as the solid bodies are assumed impenetrable in the frame of Linear Theory of Elasticity. Considering that pressure is nil outside the contact area, whereas the clearance is nil on the contact area, the boundary conditions can thus be expressed as:

$$p(x_1, x_2) \geq 0, \; h(x_1, x_2) \geq 0; \quad (2)$$

$$p(x_1, x_2) h(x_1, x_2) = 0. \quad (3)$$

The static equilibrium provides additional equations relating the unknown pressure distribution to the normal force W and its eccentricity e in the longitudinal direction x_1:

$$W = \int_{-\infty}^{\infty} \int_{-\infty}^{\infty} p(x_1, x_2) dx_1 dx_2; \quad (4)$$

$$W \cdot e = \int_{-\infty}^{\infty} \int_{-\infty}^{\infty} p(x_1, x_2) x_1 dx_1 dx_2. \quad (5)$$

The aforementioned contact model can be employed in the numerical simulation of elastic contact scenarios involving arbitrary geometry.

The difficulty in solving the contact model stems from the fact that neither the contact area, nor the pressure distribution are known in advance, and moreover, keep changing during the contact process together with the load level and the compliance of the viscoelastic material. Therefore, a trial-and-error iterative approach is adopted, which require the numerical treatment of the contact model (1) - (5).

3. MODEL DISCRETIZATION

Provided the normal displacement u_3 is accurately computed, the aforementioned contact model can also assist the numerical resolution of contact scenarios involving dissipative processes, e.g. the elastic-plastic contact, in which the development of the plastic region depends on the entire loading history [17], or the frictional

contact, in which friction as a dissipative process requires the reproduction of the loading history [18]. In these cases, the time parameter needs not be considered explicitly, as long as the contact history is properly replicated by load incrementing, assuring reproduction of the contact process path. The viscoelastic material exhibits the so-called memory effect, meaning the current state also depends upon all previous loading states, but, moreover, its elastic properties (the creep compliance or the relaxation modulus) depend explicitly on time. To overcome these dependencies, the proposed numerical solution for the viscoelastic contact model involves a spatial discretization of the contact surface, as well as a temporal discretization of the loading window.

The spatial discretization employs a rectangular uniform mesh laying in the common plane of contact, on which all problem parameters are assumed piecewise-constant, based on the discrete values computed in the mesh nodes. In this manner, the contact area is approximated by the reunion of a set of non-intersecting patches, each one supporting a uniform pressure whose magnitude is computed based on its nodal value. Mesh nodes notation can make use of discrete integers indexing the row and column grids intersecting in the corresponding patch. In the discrete model, obtaining the contact problem solution reduces to finding the magnitude of pressure in each node of the considered mesh. Problem parameters such as the rigid-body movements or the material elastic properties are independent of spatial localization.

The temporal discretization assumes that the loading window $[0,t_0]$ (where at $t=0$ the viscoelastic body was undisturbed, and t_0 is prescribed but otherwise arbitrary) is divided into small time steps. Time-dependent problem parameters, such as the discrete series of displacements and pressures, or the elastic properties of the viscoelastic material, are assumed piecewise-constant in the time dimension. On the other hand, mesh parameters such as the nodes coordinates and the mesh element sizes Δ_1 and Δ_2 remain unchanged. The notation of problem parameters can then make use of the discrete indexes, i.e. $p(i,j,k)$ is the uniform pressure predicted for the patch (i,j) of the surface spatial grid, after k time steps. The main advantage of this discretization process is the substitution of integration of arbitrary functions over arbitrary spatial or temporal domains, with summation. The latter can be performed for prescribed input, and thus favors an iterative search of the contact problem solution. The numerical approach thus circumvents the continuous integral over space and time, arising [15] in the computation of the viscoelastic displacement u_3. This further allows for an iterative solution of the contact model (1) - (5), as outlined in the following section.

4. ALGORITHM DESCRIPTION

As shown in [19], computational contact mechanics can incorporate the theory of viscoelastic behavior provided a directly additive (i.e., linear) viscoelastic response is assumed. Linearity in the stress-strain relationship of the viscoelastic material can be achieved in the framework of infinitesimal strains. While isotropic and linear elastic behavior is completely described by two material constants, the linear viscoelastic stress-strain relationship of incompressible materials employs two interchangeable functions of time, namely the relaxation modulus $\Psi(t)$ and the creep compliance $\Phi(t)$. The creep compliance function describes the viscoelastic strain response to a unit step change in stress, and the relaxation modulus, conversely, the stress response to a unit step change in strain. Assumption of incompressibility, which reduces the complexity of the constitutive law, can be considered realistic for polymers, whose Poisson's ratio usually exceeds 0.4. With these assumptions, a linear relation between the tensors of deviatoric stress s and of deviatoric strain e is established by means of the shear modulus G:

$$s = 2Ge\,, \tag{6}$$

and the linear viscoelastic strain response to arbitrary stress in the $[0,t]$ window of observation, can be expressed, according to the Boltzmann hereditary integral, by the Volterra integral equation:

$$e(t) = \int_0^t \Phi(t-t')\frac{\partial s(t')}{\partial t'}dt'\,, \tag{7}$$

In a purely elastic contact, the stress-deformation relation is based on the Green function $B(x_1, x_2)$ for the elastic half-space derived by Boussinesq, expressing the surface normal displacement induced at a point (x_1, x_2) by a concentrated normal force acting in the origin of the coordinate system. By employing the superposition principle within the linear theory of elasticity, the normal surface displacement induced by arbitrary pressure $p(x_1, x_2)$ results as:

$$u_3^{\mathrm{e}}(x_1, x_2) = \int_{-\infty}^{\infty}\int_{-\infty}^{\infty} B(x_1 - x_1', x_2 - x_2')p(x_1', x_2')dx_1'dx_2', \tag{8}$$

The viscoelastic displacement u_3^{vs} computation is achieved by substituting the elastic constant $1/(2G)$ entering the elastic displacement equation (8) with the viscoelastic creep compliance function $\Phi(t)$, as suggested in [4], and by applying the superposition implied by Volterra integral (7). The viscoelastic stress-deformation relation results as:

$$u_3^{\mathrm{vs}}(x_1, x_2, t) = 2G\int_0^t \Phi(t - t')\frac{\partial}{\partial t'}u_3^{\mathrm{e}}(x_1, x_2)dt'. \tag{9}$$

The discrete counterpart of continuous equation (8) involves the elastic influence coefficient $K_{\mathrm{e}}(i, j)$, derived as suggested in [14]:

$$u_3^{\mathrm{e}}(i, j) = \sum_{k=1}^{N_1}\sum_{\ell=1}^{N_2} K_{\mathrm{e}}(i - k, j - \ell)p(k, \ell), \quad i = 1\ldots N_1,\ j = 1\ldots N_2, \tag{10}$$

where N_1 and N_2 are the row and column number of spatial grids. By defining a viscoelastic influence coefficient:

$$K_{\mathrm{vs}}(i, j, k) = 2G\Phi(k)K_{\mathrm{e}}(i, j),\ k = 1\ldots N_t, \tag{11}$$

with N_t is the number of temporal steps, the viscoelastic displacement induced by a prescribed, but otherwise arbitrary loading history, at a prescribed time step k from the observation window, results as [15]:

$$u_3^{\mathrm{vs}}(i, j, k) = \sum_{n=1}^{k}\sum_{\ell=1}^{N_1}\sum_{m=1}^{N_2} K_{\mathrm{vs}}(i - \ell, j - m, k - n) \times \big(p(\ell, m, n) - p(\ell, m, n - 1)\big), \quad i = 1\ldots N_1,\ j = 1\ldots N_2,\ k = 1\ldots N_t, \tag{12}$$

The latter equation is the discrete counterpart of equation (9), with the viscoelastic influence coefficient $K_{\mathrm{vs}}(i - \ell, j - m, k - n)$ expressing the displacement induced after k time steps in the spatial cell (i, j), by a uniform pressure of magnitude $1/(\Delta_1\Delta_2)$ Pa, that acted in the cell (ℓ, m) in the nth time step of the observation window. Equation (12) shows that viscoelastic displacement computation requires the knowledge of all previous states.

In the discrete model, the history of pressure distribution in the viscoelastic contact is thus replicated by successively computing a pressure map for each new time increment, thus overcoming the viscoelastic memory effect. In other words, the contact model is solved successively at every time step, assuring the simulation of the loading history. The employed contact solver is based on the Conjugate Gradient-type scheme originally advanced by Polonsky and Keer [14] for the elastic contact of rough surfaces. In the beginning of the observation window, no loading history is assumed, so the initial contact state is calculated as a purely elastic process, i.e. the displacement is generated by the initial pressure only. In the subsequent time increments, the entire pressure history is used to assess the contribution of the loading history to the current displacement field, as suggested by equation (12). This contribution is superimposed in the equation of the surface of deformation (1). A similar technique was employed [17] for the contact of elastic-plastic bodies, by superimposing the residual displacement to the initial contact geometry, thus obtaining a modified hi. In this manner, the instantaneous (i.e., for a fixed, but arbitrary t) viscoelastic contact model is reduced to a purely elastic process with a modified initial contact geometry. For the latter, a robust numerical solution is readily available [14].

By solving a series of subsequent instantaneous contact states, corresponding to the discrete series of time moments considered in the temporal discretization, the simulation of the viscoelastic contact process is obtained. The flow-chart of the proposed algorithm is detailed in Fig. 1, in which the indexes for spatial localization are omitted for brevity, and the number of the time step is indicated as an upper index.

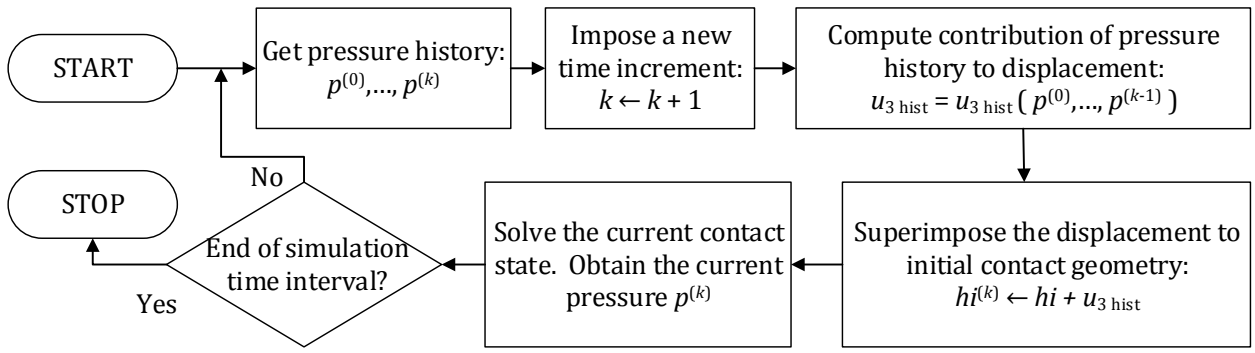

Fig. 1. Algorithm flowchart for the simulation of the loading history.

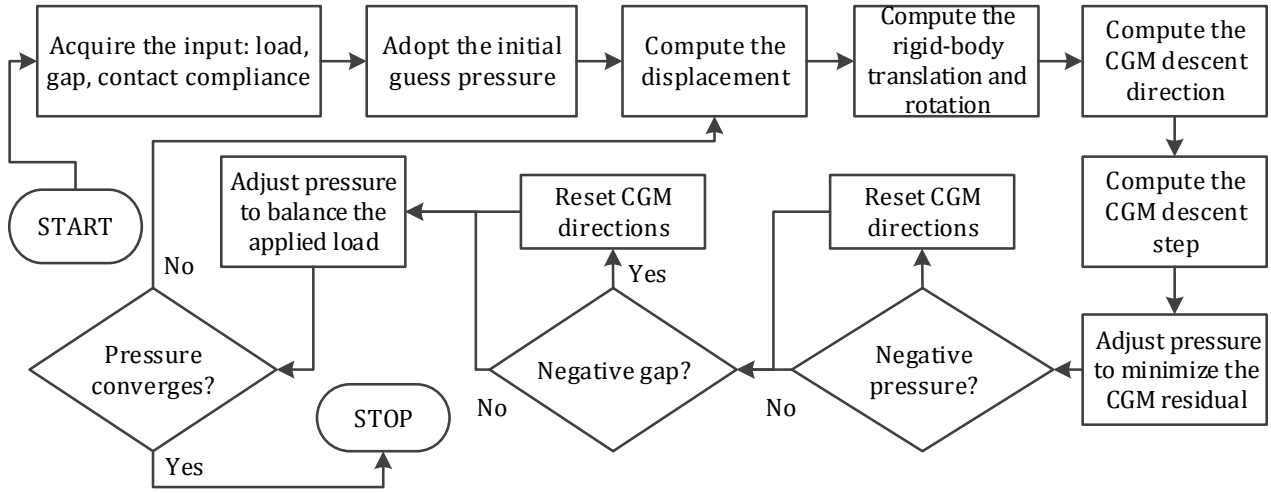

Fig. 2. Algorithm flowchart for solving the instantaneous contact state.

The instantaneous contact area and pressure distribution are determined with a trial-and-error approach, as suggested in [14]. A guess contact region is assumed, and the pressure distribution is then iterated based on this assumption. The iteration implies the repeated resolution of the linear system resulting from equation (1), having the nodal pressures as unknowns. The Conjugate Gradient Method (CGM) is employed, due to its superlinear rate of convergence. The convergence of the CGM can is guaranteed as the influence coefficients matrix, matching the system matrix, is symmetric and positive definite. Additional constraints resulting from equations (4) and (5) are applied at each iteration of the CGM, whereas the violation of the boundary conditions (2) and (3) results in a reinitialization of the residual minimization path in the CGM by a reset of the conjugate directions. When all constraints in the contact model (1) - (5) are verified, a contact problem solution is achieved. This solution is unique based on the theorem of uniqueness of solution of the elastostatic problem. Otherwise, the process is restarted with a different initial guess. An outline of the employed algorithm to obtain the instantaneous contact state is depicted in Fig. 2. A detailed description of the algorithm for solving the frictionless elastic contact problem is beyond the point of this paper, but an interested reader is redirected to the algorithm [20] for the slip-stick elastic contact, which features a general solution for the elastic contact involving all types of rigid-body translations and rotations.

The algorithmic computational complexity is dictated by the number of nodes in the spatial mesh, i.e. $N_1 \times N_2$, as well as by the number of temporal steps N_t. The most computationally intensive operations are the convolution products related to the superposition of pressure effects in the two spatial dimensions. The computational impact is dramatic because these convolutions must be computed two times per iteration in the CGM. The correlation between the density in the spatial mesh and the precision goals of the CGM was discussed in [14].

The discrete convolution calculations can be accelerated by employing the Discrete Convolution fast Fourier transform (DCFFT) [21,22], leading to a decrease in the computational complexity from $O(N_1^2 N_2^2)$ to $O(N_1 N_2 \log(N_1 N_2))$ per time step. The DCFFT exploits a remarkable property of the convolution product, namely that it can be calculated as an element-wise product in the Fourier transform domain. The practice of numerical simulation applied to finite length line contacts suggests adoption of a spatial mesh with a variable step size, with higher density of nodes towards the roller end, where pressure risers are expected due to the singularity in the punch ordinate. Such meshing techniques are not compatible, however, with the DCFFT, which requires the mesh to be uniform. It should be remembered that the influence coefficients depend on the distance between the observation and the excitation point, and a variable-step size would increase considerably the overall number of possible distances between the mesh nodes.

Considering that equation (12) is a 2D discrete convolution product in the space dimension but not in the time dimension, the order of computations for the entire simulation window results as $O(N_t^2 N_1 N_2 \log(N_1 N_2))$. The numerical simulations performed with the newly proposed computer program suggests that mesh convergence can be achieved with a relatively small number of time steps. Practically, a contact simulation performed on a spatial mesh with 2^{18} nodes and with 120 time steps was finished on a 4-core 3.2 GHz CPU in less than 15 minutes. It should be noted that the computation of the 3D array of influence coefficients only needs to be performed once.

5. VISCOELASTIC FINITE LENGTH LINE CONTACT

In a finite length line contact, the theoretical models predict an infinite pressure at the sharp edge of the shorter contacting body. However, in practice, plastic yielding or inherent errors in the manufacturing process limit the contact stresses to a finite, yet large, value. Highly localized stress concentrations induced by the pressure risers pose a major threat to the load carrying capacity of the contact, and therefore the reduction of these end effects was the subject of numerous research efforts [1-3].

Comparison of various profiling techniques requires numerical simulation [2,3]. However, there exist a major disadvantage in treating the problem numerically: uniform grids are not performing optimally in finite length line contact analysis. Both pressure and width of contact area are weak functions of the longitudinal coordinate in the central region, where the Hertz theory may apply, but vary significantly toward the ends, where the gradient of pressure increases abruptly. The peak pressure value is very sensitive to discretization. The contact area manifests enlargements at the ends, which are referred to as a “dog bone” shape [19].

The case of contacting cylinders of the same length cannot be solved in the frame of the half-space approximation, and therefore is beyond the scope of this paper. When one contacting cylinder is sufficiently shorter, the other body can be treated as an elastic half-space. Therefore, in this paper, the contact between a rigid cylindrical indenter and a viscoelastic half-space is considered. If the indenter is not rounded, a singularity in the contact stress is expected. Considering that the numerical technique averages pressure over each contact patch, such singularities can only be described in an approximate manner.

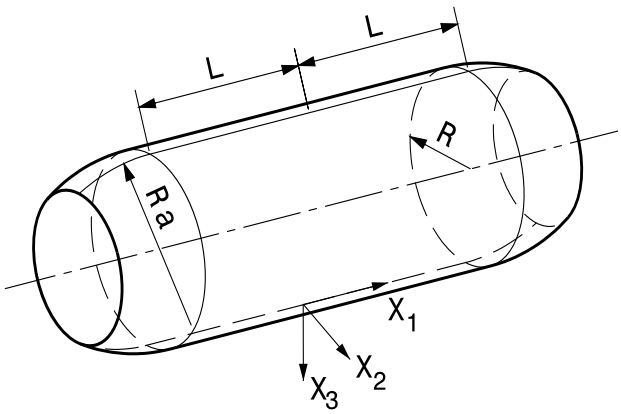

Fig. 3. The geometry of the indenter.

In this paper, a rounding radius is introduced, i.e., partial crowning [2], to minimize this disadvantage. The crowning arc, of radius R_a, is assumed tangent to the linear portion of the roller generatrix, of half-length L, as depicted in Fig. 3. The roller radius in the unprofiled region is denoted by R. The indenter geometry results as:

$$hi(x_1, x_2) = \begin{cases} R - \sqrt{R^2 - x_2^2}, & |x_1| \le L \\ R - \sqrt{\left[R_a - R - \sqrt{R_a^2 - (x_1 - L \cdot \mathrm{sgn}(x_1))^2}\right]^2 - x_2^2}, & |x_1| > L \end{cases} \quad (13)$$

The load level is chosen so that the contact area half-length does not approach the roller's end, i.e. there exist sufficient material around the contact to provide support, as shown in Fig. 4.

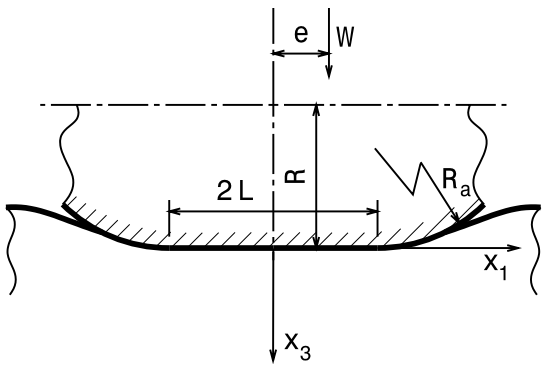

Fig. 4. Contact geometry after deformation.

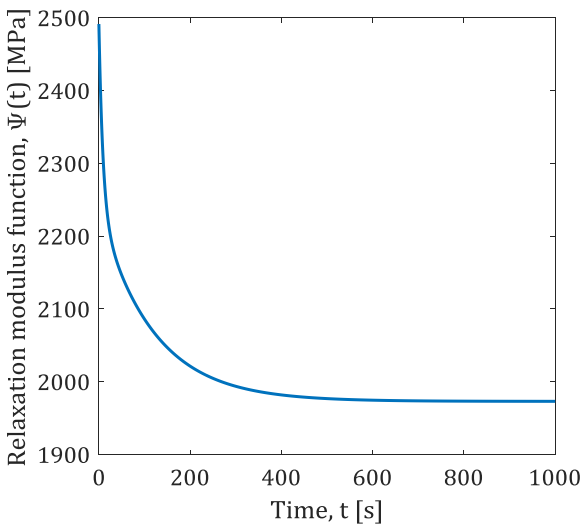

Fig. 5. Relaxation modulus function of PMMA.

The constitutive law of the viscoelastic material employed in this paper is that of the polymethyl methacrylate (PMMA), a thermoplastic polymer whose relaxation modulus under uniaxial compression was obtained experimentally by Kumar and Narasimhan [23]. Figure 5 depicts the measured data in a window of observation of 1000 s. The relation between the creep compliance and the relaxation modulus function in the Laplace transform domain, i.e.:

$$\bar{\Psi}(s)\bar{\Phi}(s) = 1/s^2, \quad (14)$$

can be further used to derive the creep compliance of PMMA by inverse Laplace transform, yielding:

$$\Phi(t) = 7 \cdot 10^{-4} - 6.17 \cdot 10^{-5} \exp(-0.1t) - 8.38 \cdot 10^{-5} \exp(-7.47 \cdot 10^{-3} t), \ [1/\mathrm{MPa}]. \quad (15)$$

It should be noted that in the time domain the creep compliance and relaxation modulus functions are not reciprocal like in the purely elastic case, i.e. $\Psi(t)\Phi(t) \neq 1$.

6. RESULTS AND DISCUSSIONS

The computer program was first benchmarked against the implicit solutions derived in the classical literature [4-8] of the viscoelastic contact for the step loading spherical indentation of a viscoelastic half-space described by the Maxwell or Zener rheological model. The Hertz (i.e., at $t = 0$) contact parameters, namely the contact radius a_H and the central pressure p_H, are used as normalizers in Figs. 6 and 7, depicting the radial pressure distributions achieved at various time moments from the loading history. A good agreement with the classic solution is found. The latter solution, detailed in Appendix, requires further numerical treatment, and is valid for monotonically increasing contact radius only. The predictions of the proposed computer program are depicted using dashed lines, whereas the data resulting from the classic framework is displayed with continuous lines in Figs. 6 and 7.

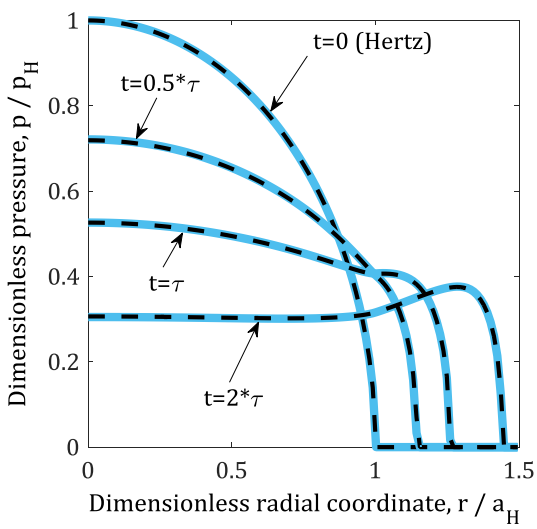

Fig. 6. A Maxwell half-space spherical indentation.

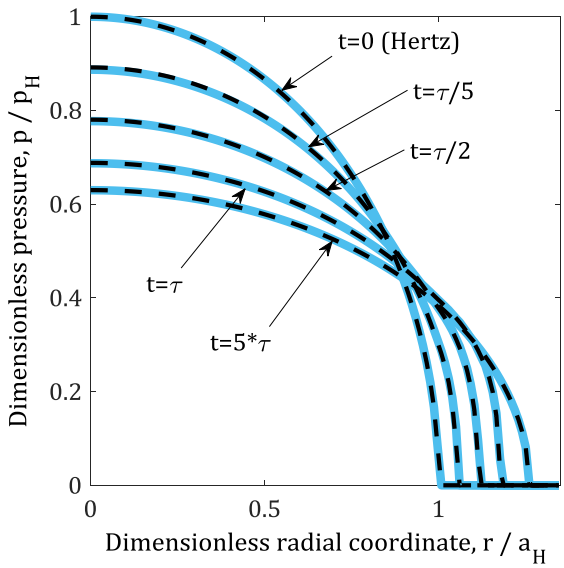

Fig. 7. A Zener half-space spherical indentation.

The finite length line contact of viscoelastic materials is studied by pressing a rigid roller whose contact geometry is described by equation (13), into a viscoelastic PMMA half-space of the creep compliance given in equation (15) and of Poisson's ratio $\nu = 0.38$ [23].

A step-loading $W(t) = W_0 H(t)$ is assumed, where $H(t)$ denotes the Heaviside step function, and $W_0 = 10\,\text{kN}$. In this study, the Poisson's ratio of the viscoelastic material is assumed constant with time, and consequently the relaxation functions in response to volumetric and shear deformations are in a fixed ratio [19].

In this manner, the assumption of material incompressibility can be discarded [19]. The roller dimensions are [2]: $2L = 19.13\,\text{mm}$, $R_a = 7500\,\text{mm}$, $R = 5\,\text{mm}$. Figures 8-10 describe the centric loading, and therefore only one fourth of the spatial computational domain is depicted, due to symmetry; whereas, in case of eccentric loading, one half is retained.

Iso-contours of centric pressure distribution predicted for $t = 240\,\text{s}$ are depicted in Fig. 8, whereas Figs. 9 and 10 show the extents of the contact area and the longitudinal pressure profiles, respectively, at different moments from the loading history.

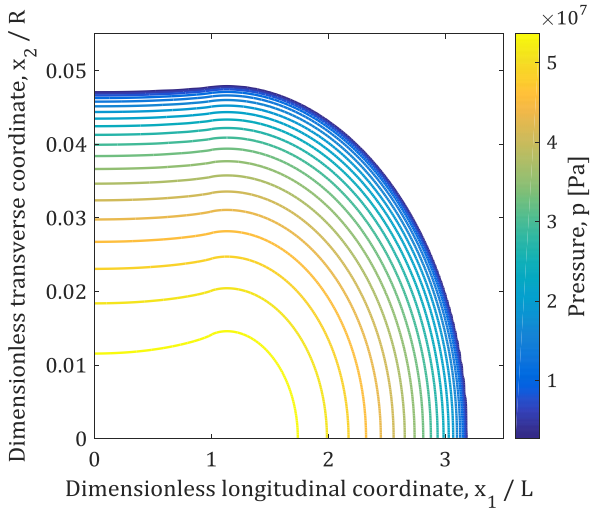

Fig. 8. Pressure iso-contours, $t = 240\,\text{s}$, $e = 0$.

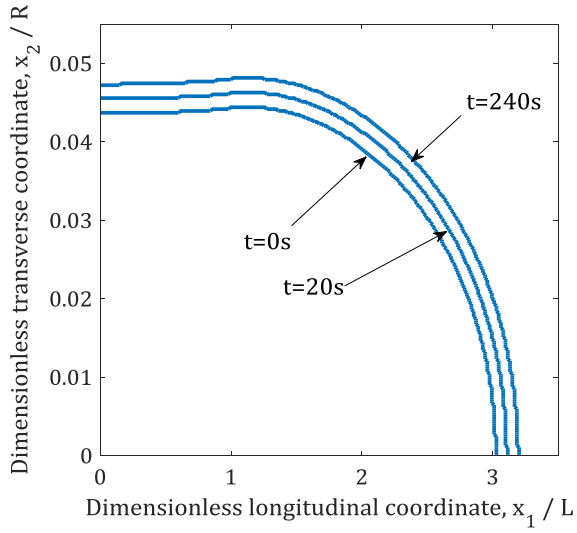

Fig. 9. Contact area extents, $e = 0$.

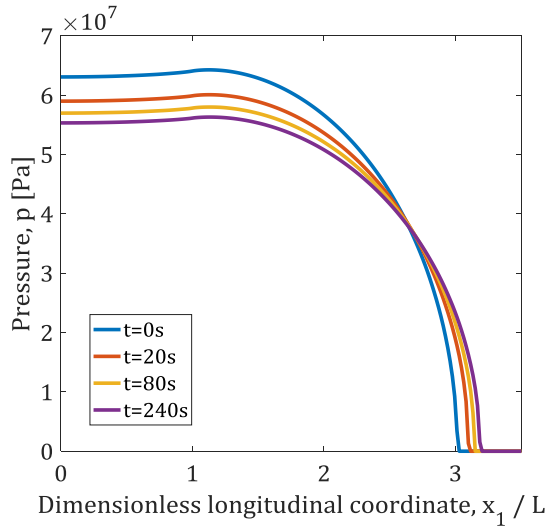

Fig. 10. Longitudinal pressure profiles, $e = 0$.

As in the case of the spherical contact, the contact area grows with time, leading to shallower pressure in the regions of the initial contact surface. Subsequent contact area boundaries in Fig. 9 follow the initial "dog bone" shape, well known from the theory of the elastic finite length line contact. The longitudinal pressure profiles display a pressure riser related to the end effect, whose intensity diminishes with time, as shown in figure 10. The choice of the crowning radius R_a has a chief influence on this riser.

Considering the stabilization in the PMMA compliance suggested in Fig. 5 after $t \cong 250$ s, the contact parameters are not expected to vary significantly. It should be noted that these findings apply to PMMA only, other constitutive laws may lead to different contact behaviours.

The practical applications of the finite length line contact may involve an a priori unknown misalignment, i.e. an angular displacement of the roller axis with respect to the shaft axis, measured in the plane defined by the applied load vector and the shaft axis. The latter situation can be treated by assuming a force eccentricity, leading to a non-symmetric pressure distribution whose resultant is shifted to compensate for the resulting tilting moment. The predicted contact parameters are depicted in figures 11-13 for $e/L = 0.5$, and in Figs. 14-16 for $e/L = 1$.

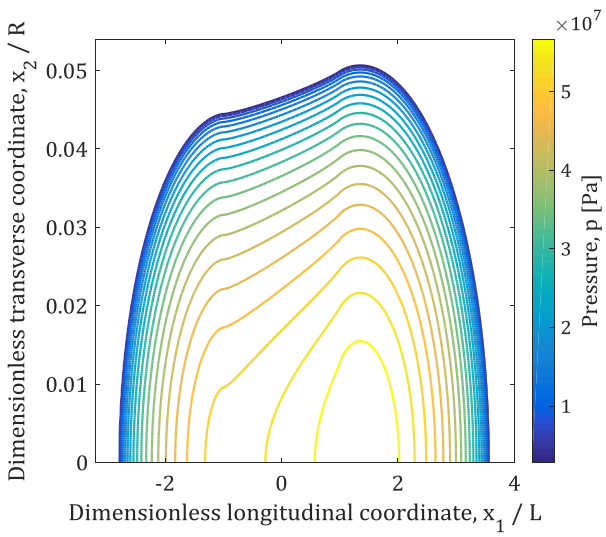

Fig. 11. Pressure iso-contours, $t = 240$ s, $e/L = 0.5$.

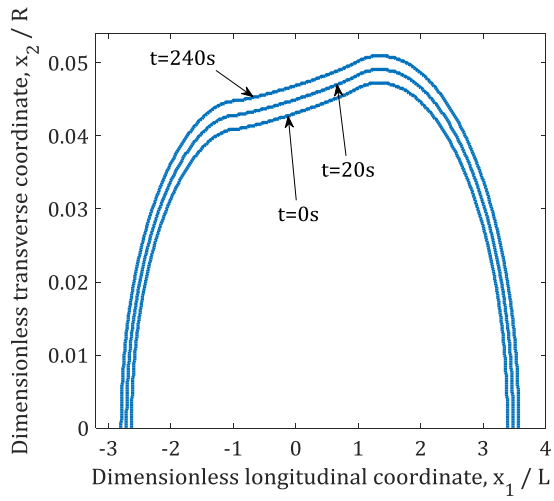

Fig. 12. Contact area extents, $e/L = 0.5$.

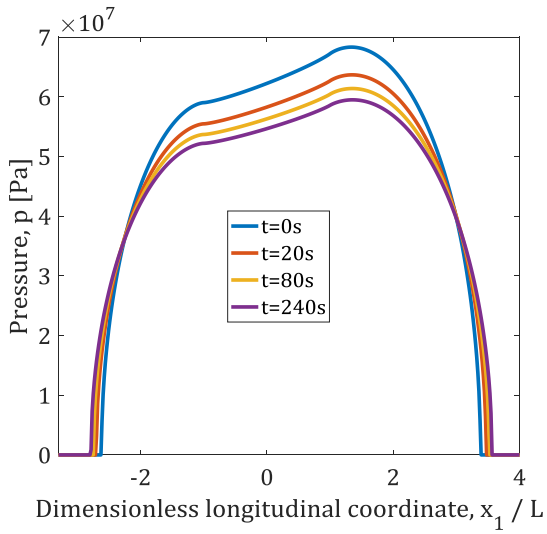

Fig. 13. Longitudinal pressure profiles, $e/L = 0.5$.

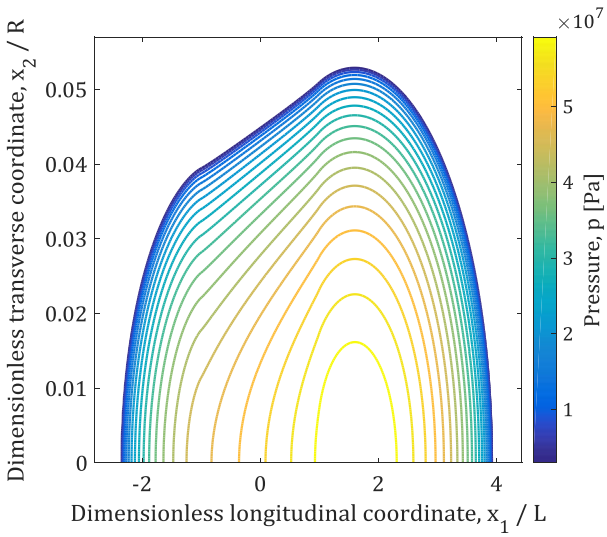

Fig. 14. Pressure iso-contours, $t = 240$ s, $e/L = 1$.

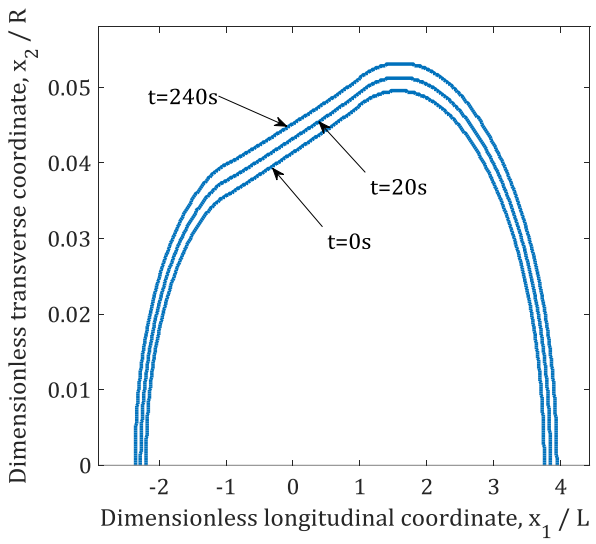

Fig. 15. Contact area extents, $e/L=1$.

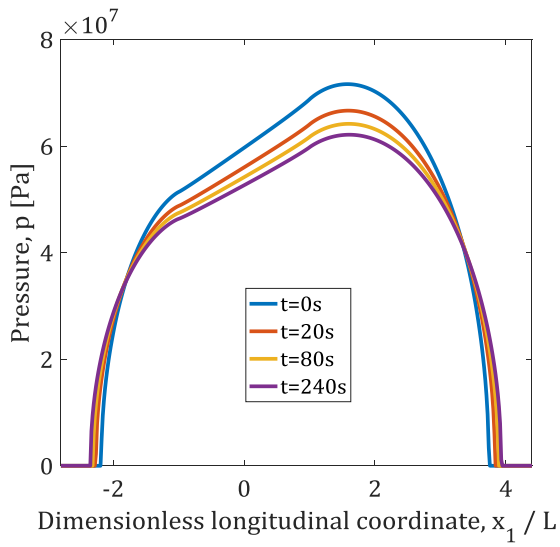

Fig. 16. Longitudinal pressure profiles, $e/L=1$.

The progress with time of the eccentric contact process bear similarities with the centric case. An additional inclination in the longitudinal pressure profiles can be found, as in Figs. 13 and 16, accompanied by a widening of the contact area in the direction of the force eccentricity, as suggested in Figs. 12 and 15. A diminishing in the opposite pressure riser is predicted with increasing e, as shown in Fig. 14, as the roller tilting brings less of the profiled region into contact.

The variation with time of the contact area, the tilting angle and the rigid-body approach, for various eccentricities are depicted in Figs. 17, 18 and 19, respectively. The contact area and the normal approach follow a similar trend, dictated by the relaxation modulus function of the viscoelastic material (Fig. 5). Numerical oscillations can be seen in Fig. 17 as jagged lines, caused by the assumption of a discrete contact area calculated as the sum of areas of elementary cells having a small, but non-vanishing, magnitude. In the numerical approach, the contact area can only vary in increments equal to the area of the elementary patch, multiplied by the number of axes of symmetry. These oscillations can be reduced by employing finer spatial meshes. The performed numerical simulations suggest that higher eccentricity lead to smaller contact area and rigid-body approach, but to higher tilting angle and pressure riser in the eccentricity direction. The data depicted in Fig. 18 shows that the growing tilting angle has an initial rapid variation, then increases monotonically at a small rate.

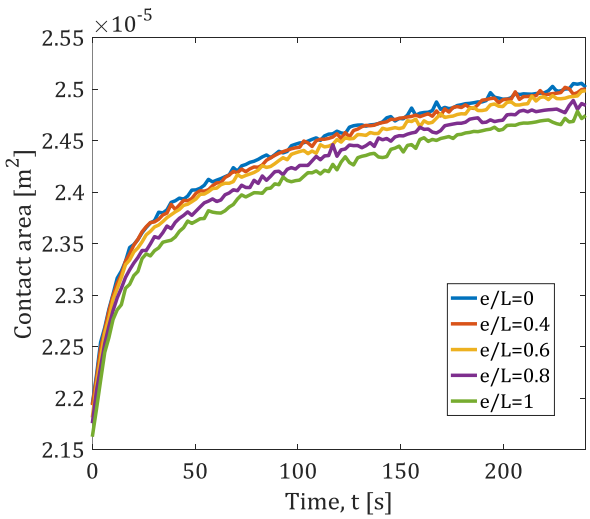

Fig. 17. Contact area vs. time, various eccentricities.

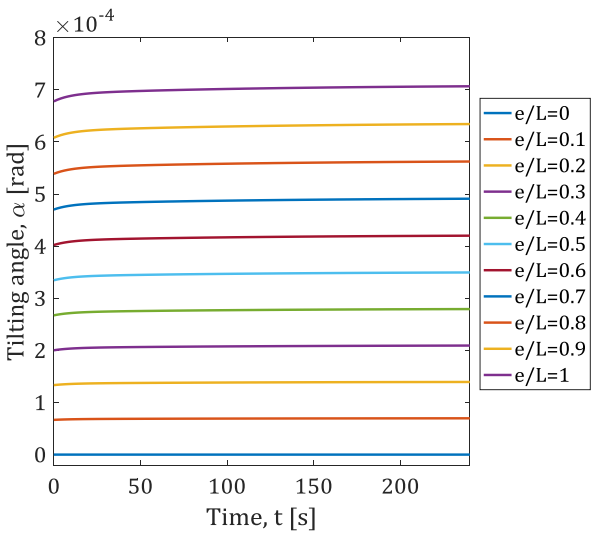

Fig. 18. Tilting angle vs. time, various eccentricities.

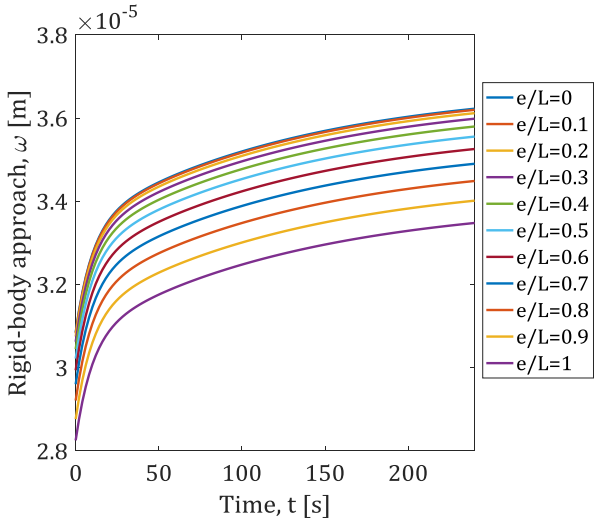

Fig. 19. Rigid-body approach vs. time, various eccentricities.

Although the contact geometry was chosen considering practical applications, the presented simulations prove the model ability to treat various contact processes involving the finite length line contact of linear viscoelastic materials. The literature of the finite length elastic contact has proven [1-3] that small changes in the roller profile may significantly disturb the contact stresses, making the contact problem ill-conditioned. This is especially true for the profiling radius R_a, whose choice has a chief influence on the resulting pressure riser. A smaller radius may result in important gradients of pressure, leading to subsurface stress concentrations that favor plastic yielding and crack nucleation, negatively affecting the service life of the contacting element.

7. CONCLUSIONS

The simulation of the finite length line contact of linear viscoelastic materials is achieved in this paper by combining a solver for the frictionless elastic normal contact with a numerical method for the calculation of the displacement induced in a viscoelastic half-space by a prescribed but otherwise arbitrary pressure history. Due to the robustness of the contact solver, tilting angles induced by force eccentricity can also be predicted.

The strong points of the newly proposed algorithm consist in:

1. the ability to incorporate complex models of viscoelasticity, including discrete data resulting from experimental measurements, without the need for further interpolation/regression;
2. the capability to treat arbitrary contact geometry, including mapped surfaces measured by 3D surface imaging devices (optical profilometers, atomic force microscopes etc.);
3. the ability to replicate the contact process for prolonged periods of time, due the increased computational efficiency of the convolution products calculation, and
4. the capacity to simulate arbitrary loading histories (including unloading breaks), without the drawbacks of the classic solution of the viscoelastic contact, requiring numerous conditional statements, as well as resolution of transcendental equations.

Comparison with results for the spherical contact of viscoelastic materials described by classic rheological models provides program validation. The numerical simulation technique is employed to predict the evolution of contact parameters in the finite length line contact of viscoelastic materials subjected to centric or eccentric loading. The presented simulation results prove the method ability to tackle complicated contact problems arising in practical engineering applications but lacking analytical solution.

Acknowledgement

This work was partially supported from the project "Integrated Center for Research, Development and Innovation in Advanced Materials, Nanotechnologies, and Distributed Systems for Fabrication and Control", Contract No. 671/09.04.2015, Sectoral Operational Program for Increase of the Economic Competitiveness co-funded from the European Regional Development Fund.

REFERENCES

[1] G. Lundberg, A. Palmgren, *Dynamic Capacity of Rolling Bearings*, Stockholm Royal Swedish Academy of Engineering Sciences, 1952.

[2] M.J. Hartnett, *The Analysis of Contact Stresses in Rolling Element Bearings*, Journal of Lubrication

Technology, vol. 101, iss. 1, pp. 105-109, 1979, doi: 10.1115/1.3453270

[3] J.M. de Mul, J.J. Kalker, B. Fredriksson, *The Contact Between Arbitrarily Curved Bodies of Finite Dimensions*, Journal of Tribology, vol. 108, iss. 1, pp. 140-148, 1986, doi: 10.1115/1.3261134

[4] E.H. Lee, J.R.M. Radok, *The Contact Problem for Viscoelastic Bodies*, Journal of Applied Mechanics, vol. 27, iss. 3, pp. 438-444, 1960, doi: 10.1115/1.3644020

[5] S.C. Hunter, *The Hertz Problem for a Rigid Spherical Indenter and a Viscoelastic Half-Space*, Journal of the Mechanics and Physics of Solids, vol. 8, iss. 4, pp. 219-234, 1960, doi: 10.1016/0022-5096(60)90028-4

[6] W.H. Yang, *The Contact Problem for Viscoelastic Bodies*, Journal of Applied Mechanics, vol. 33, iss. 2, pp. 395-401, 1966, doi: 10.1115/1.3625055

[7] T.C.T Ting, *The Contact Stresses Between a Rigid Indenter and a Viscoelastic Half-Space*, Journal of Applied Mechanics, vol. 33, iss. 4, pp. 845-854, 1966, doi: 10.1115/1.3625192

[8] T.C.T. Ting, *Contact Problems in the Linear Theory of Viscoelasticity*, Journal of Applied Mechanics, vol. 35, iss. 2, pp. 248-254, 1968, doi: 10.1115/1.3601188

[9] E.H. Lee, *Stress Analysis in Visco-Elastic Bodies*, Quarterly of Applied Mathematics, vol. 13, pp. 183-190, 1955, doi: 10.1090/qam/69741

[10] J.R.M. Radok, *Visco-Elastic Stress Analysis*, Quarterly of Applied Mathematics, vol. 15, pp. 198-202, 1957, doi: 10.1090/qam/92453

[11] W.W. Chen, Q.J. Wang, Z. Huan, X. Luo, *Semi-Analytical Viscoelastic Contact Modeling of Polymer-Based Materials*, Journal of Tribology, vol. 133, iss. 4, pp. 041404–1-10, 2011, doi: 10.1115/1.4004928

[12] I.F. Kozhevnikov, D. Duhamel, H.P. Yin, Z.-Q. Feng, *A New Algorithm for Solving the Multi*-Indentation *Problem of Rigid Bodies of Arbitrary Shapes on a Viscoelastic Half-Space*, International Journal of Mechanical Sciences, vol. 52, iss. 3, pp. 399-409, 2010, doi: 10.1016/j.ijmecsci.2009.10.015

[13] K.E. Koumi, T. Chaise, D. Nelias, *Rolling Contact of a Rigid Sphere/Sliding of a Spherical Indenter Upon a Viscoelastic Half-Space Containing an Ellipsoidal Inhomogeneity*, Journal of the Mechanics and Physics of Solids, vol. 80, pp. 1-25, 2015, doi: 10.1016/j.jmps.2015.04.001

[14] I.A.Polonsky, L.M. Keer, *A Numerical Method for Solving Rough Contact Problems Based on the Multi-Level Multi-Summation and Conjugate Gradient Techniques*, Wear, vol. 231, iss. 2, pp. 206-219, 1999, doi: 10.1016/S0043-1648(99)00113-1

[15] S. Spinu, D. Gradinaru, Semi-*Analytical Computation of Displacement in Linear Viscoelastic Materials*, IOP Conference Series: Materials Science and Engineering, vol. 95, 2015, pp. 012111–1-7, doi: 10.1088/1757-899X/95/1/012111

[16] J.J. Kalker, Y. Van Randen, *A Minimum Principle for Frictionless Elastic Contact with Application to Non-Hertzian Half-Space Contact Problems*, Journal of Engineering Mathematics, vol. 6, iss. 2, pp. 193-206, 1972, doi: 10.1007/BF01535102

[17] C. Jacq, D. Nélias, G. Lormand and D. Girodin, *Development of a Three-Dimensional Semi-Analytical Elastic-Plastic Contact Code*, Journal of Tribology, vol. 124, iss. 4, pp. 653-667, 2002, doi: 10.1115/1.1467920

[18] S. Spinu, G. Frunza, *The Hysteretic Behaviour of Partial Slip Elastic Contacts Undergoing a Fretting Loop*, Journal of Physics: Conference Series, vol. 585, pp. 012007–1-8, 2015, doi: 10.1088/1742-6596/585/1/012007

[19] K.L. Johnson, *Contact Mechanics*, Cambridge University Press, Cambridge, 1985.

[20] S. Spinu, D. Amarandei, *Numerical Simulation of Slip-Stick Elastic Contact*, in M. Andriychuk (Ed.): Numerical Simulation, IntechOpen, pp. 129-154, 2012, doi: 10.5772/48451

[21] S.B. Liu, Q. Wang, G. Liu, *A Versatile Method of Discrete Convolution and FFT (DC-FFT) for Contact Analyses*, Wear, vol. 243, iss. 1-2, pp. 101-111, 2000, doi: 10.1016/S0043-1648(00)00427-0

[22] S. Liu, Q. Wang, *Studying Contact Stress Fields Caused by Surface Tractions With a Discrete Convolution and Fast Fourier Transform Algorithm*, Journal of Tribology, vol. 124, iss. 1, pp. 36-45, 2001, doi: 10.1115/1.1401017

[23] M.V.R Kumar, R. Narasimhan, *Analysis of Spherical Indentation of Linear Viscoelastic Materials*, Current Science, vol. 87, no. 8, pp. 1088-1095, 2004.

APPENDIX

The classic literature of the viscoelastic contact provides implicit relations for the solution of the axisymmetric contact involving linear viscoelastic materials. These solutions often require further numerical treatment, such as numerical integration and differentiation. Moreover, when the contact radius is not increasing monotonically,

the solution of transcendental equations is also needed. Particularization of the general relations for the monotonically increasing contact area in the point contact of viscoelastic materials whose constitutive law is described by basic rheological models, subjected to step loading, lead to the contact solution presented in Table 1. For both Maxwell and Zener units, the contact radius can be expressed as:

$$a(t) = \sqrt[3]{3RW_0\Phi(t)/8}\,, \qquad (16)$$

where R is the radius of the spherical indenter, and $\Phi(t)$ the creep compliance function. The latter depends on the characteristic parameters of the basic rheological units: G - the elastic modulus of the purely elastic springs governed by Hooke's law, and η - the coefficient of viscosity of purely viscous dampers, acting as Newtonian fluids.

Table 1. The solution of step loading spherical indentation for the Maxwell and Zener rheological models.

Rheological model	Creep compliance	Radial pressure distribution
Maxwell 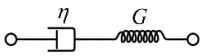	$\Phi(t) = \frac{1}{2G}\left(1+\frac{t}{\tau}\right)$ $\tau = \eta/G$	$p(t,r) = \frac{8G}{\pi R}\left(\left(a(t)^2 - r^2\right)^{\frac{1}{2}} - \frac{1}{\tau}\int_0^t \exp\left(\frac{t'-t}{\tau}\right)\mathrm{Re}\left(\left(a(t')^2 - r^2\right)^{\frac{1}{2}}\right)dt'\right)$
Zener 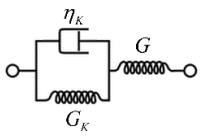	$\Phi(t) = \frac{1}{2}\left(\frac{1}{G} + \frac{1-\exp(-t/\tau)}{G_\mathrm{K}}\right)$ $\tau = \eta_\mathrm{K}/G_\mathrm{K}$	$p(t,r) = \frac{8G}{\pi R}\left(\left(a(t)^2 - r^2\right)^{\frac{1}{2}} - \frac{1}{\tau}\int_0^t \exp\left(\frac{2(t'-t)}{\tau}\right)\mathrm{Re}\left(\left(a(t')^2 - r^2\right)^{\frac{1}{2}}\right)dt'\right)$